space available to us. (For this reason we could not use conventional slots.)

The ring-loaded slot is also a structure amenable to accurate analysis by mode-matching methods [4, 5]. Using the same numerical optimization procedure as before, we were able to design a satisfactory bandstop filter; Figure 2 shows that an additional ~ 30 dB of isolation was achieved in the vicinity of 10.8 GHz, and the passband of 8–8.4 GHz was not significantly affected.

The combined bandpass/bandstop waveguide filter was then fully analyzed by the mode-matching method. The advantage of being able to calculate the filter characteristics accurately is that one can have a definitive design before manufacture. In addition, by making small perturbations to the parameters of the final design, the manufacturing tolerances required to ensure the desired performance can be readily established. In our design, analysis showed that the filter should be machined within ± 0.05 mm of the given dimensions in order to achieve the predicted filter characteristics satisfactorily.

3. RESULTS

With these tolerances in mind, the combined filter, shown in Figure 3(a), was constructed and its performance accurately measured on a network analyzer. The comparison with the predicted values is shown in Figure 3(b). As can be seen, the agreement is quite remarkable, even down to the fine structure of the filter characteristic at the −30 to −40-dB levels. This result demonstrates what can be achieved when accurate theoretical modeling is combined with high-quality manufacturing. Indeed, without both of these capabilities, it is difficult to see how an effective filter could have been developed.

4. CONCLUSION

We have described a multi-iris bandpass filter used in conjunction with a ring-loaded slot bandstop filter in circular waveguide. The addition of the ring-loaded slot bandstop filter provides a considerable band of high attenuation and improved stop-band performance beyond what is possible with the multiiris bandpass filter alone. Our computer analysis shows excellent agreement when compared with the measured data.

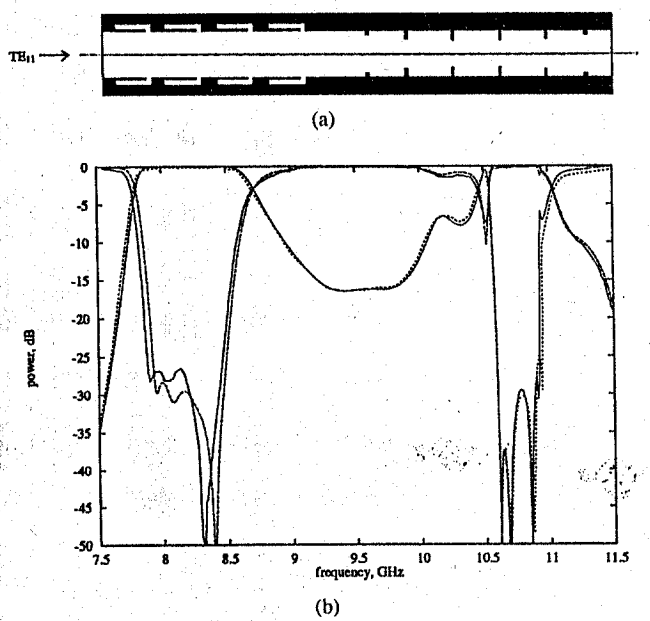

Figure 3 Combined bandpass/bandstop X-band filter in circular waveguide. (a) Cross-sectional view of the filter. (b) Calculated and measured return and transmission loss of the filter response. Solid line, measured return loss; long-dashed line, predicted; short-dashed line, measured transmission; dotted line, predicted

REFERENCES

1. J. Bornemann and F. Arndt, "Metal-Insert Filters with Improved Characteristics," *IEEE Proc. Pt. H*, Vol. 133, No. 2, 1986, pp. 103–107.
2. G. L. James, "Analysis and Design of TE_{11}-to-HE_{11} Corrugated Cylindrical Waveguide Mode Converters," *IEEE Trans. Microwave Theory Tech.*, Vol. MTT-29, 1981, pp. 1059–1066.
3. J. W. Bandler and C. Charalambous, "Practical Least *p*th Optimization of Networks," *IEEE Trans. Microwave Theory Tech.*, Vol. MTT-20, 1972, pp. 834–840.
4. G. L. James and B.MacA. Thomas, "TE_{11} to HE_{11} Cylindrical Waveguide Mode Converters Using Ring-Loaded Slots," *IEEE Trans. Microwave Theory Tech.*, Vol. MTT-30, 1982, pp. 278–285.
5. E. Kühn and V. Hombach, "Computer-Aided Analysis of Corrugated Horns with Axial or Ring-Loaded Slots," in *Proc. ICAP83*, pp. 127–131.

Received 10-20-94

Microwave and Optical Technology Letters, 8/5, 229–230

CCC 0895-2477/95

MODE DEGENERACY IN QUASIOPTICAL RESONATORS

G. P. Monahan, P. L. Heron, and M. B. Steer
Research Electronics Laboratory
Department of Electrical and Computer Engineering
North Carolina State University
Raleigh, North Carolina 27695

J. W. Mink*
United States Army Research Office
Research Triangle Park
North Carolina 27709

F. K. Schwering
CECOM, Attn. AMSEO-RD-C3-D
Fort Monmouth, New Jersey 07703

ABSTRACT

Fabry-Perot resonators and beam waveguides are used in quasioptical systems to refocus electromagnetic fields. These fields are described by Laguerre Gaussian or Hermite Gaussian quasi-TEM mode families depending on whether the aperture is rectangular or circular. It is shown that certain lower-order Laguerre Gaussian and Hermite Gaussian modes are identical. This has implications for the design of quasioptical systems for mode selection. © 1995 John Wiley & Sons, Inc.

I. INTRODUCTION

Fabry-Perot resonators and beam waveguides are used in quasioptical systems such as power combiners, amplifiers, and frequency multipliers. Successful implementation of these structures in quasioptical systems requires an understanding of the mode structures they support. This article presents the classical development of the modal fields of Fabry-Perot

* He is now with North Carolina State University.

resonators. As usual these are approximated as either Hermite Gaussian (HG) or Laguerre Gaussian (LG) mode families; which exists is usually thought to be determined by whether the aperture is rectangular or circular, respectively. For the first time the approximated mode families are derived using common terminology. A surprising result is that the lower-order modes of the respective mode families are identical. This considerably simplifies the design of quasioptical system components, as only one set of mode families needs to be considered and the higher-order modes are easily suppressed.

II. FIELD STRUCTURE

A Fabry-Perot resonator typically has two spherical section reflectors that may be of either rectangular or circular aperture, as shown in Figure 1. Using Huygen's principle [1, 2] the traveling-wave electric field (E) on one of the surfaces (S) of the resonator can be found from the sum of the contributions of the traveling-wave electric field (E') on the surface of the opposite reflector (S'), as given by the integral:

$$E = \int_{S'} \frac{jk(1+\cos\theta)}{4\pi R} e^{-jkR} E'\, dS', \tag{1}$$

where $R = |\mathbf{R}|$ and $\mathbf{R}$ is the vector from a point on S' to a point on S, and θ is the angle between the surface normal of S' and $\mathbf{R}$. In a Fabry-Perot resonator the field on one mirror reproduces itself on the opposite mirror with a complex proportionality factor σ, so that $E = \sigma E'$ and

$$E = \sigma \int_{S'} \frac{jk(1+\cos\theta)}{4\pi R} e^{-jk} E\, dS'. \tag{2}$$

III. MODE ANALYSIS

Solution of (2) yields both the field structure and the diffraction loss. Unfortunately, it must be solved numerically, and so approximations [1, 2] are used to develop modal field descriptions. Closed-form solutions to (2) can be found after making appropriate approximations. A near-field polynomial approximation for R is used in the exponential term, and a far-field approximation for R is used in the denominator term. Unity is used to approximate $\cos\theta$. For circular aperture resonators, circular cylindrical coordinates (r, ϕ, z) are used, while Cartesian coordinates (x, y, z) are used for rectangular apertures. Using the approximations, the solution to (2) for circular apertures is given by

$$\begin{aligned} \mathrm{LG}_{pt} &= \frac{E(r,\phi,\pm d/2)_{p,t}}{E_0} \\ &= N_{lg}(p,t)\left(\frac{r\sqrt{2}}{w_s'}\right)^t L_p^t\left(\frac{2r^2}{w_s'^2}\right) \\ &\quad \times \exp\left[\frac{-r^2}{w_s'^2}\right]\begin{pmatrix}\cos(t\phi)\\ \sin(t\phi)\end{pmatrix}. \end{aligned} \tag{3}$$

Using the same approximations in rectangular coordinates, the solution for a rectangular aperture is given by

$$\begin{aligned} \mathrm{HG}_{mn} &= \frac{E(x,y,\pm d/2)_{m,n}}{E_0} \\ &= N_{hg}(n,m) H_m\left(\frac{x\sqrt{2}}{w_s'}\right) H_n\left(\frac{y\sqrt{2}}{w_s'}\right) \\ &\quad \times \exp\left[\frac{-(x^2+y^2)}{w_s'^2}\right], \end{aligned} \tag{4}$$

where m, n, p, and t are the mode indices corresponding to the x, y, r, and ϕ directions, respectively; $N_{hg}(n,m)$ and $N_{lg}(p,t)$ are normalizing coefficients for the HG and LG modes, respectively; $H_m(X)$ is the Hermite polynomial defined by the Rodrigues formula, $H_m(X) = (-1)^m e^{-X^2} d^m e^{-X^2}/dX^m$ [3]; $L_p^t(R)$ is the generalized Laguerre polynomial; the spot size at the reflectors is

$$w_s' = \sqrt{\frac{\lambda b'}{\pi}}\left(\frac{d}{2b'-d}\right)^{1/4}, \tag{5}$$

where λ is the wavelength; b' is the resonator radius of curvature; and d is the resonator spacing.

Note that aperture dimensions affect the losses, which are quantified by σ and can only be found through numerical solution of (2). Analyzing the losses as a function of mode number and frequency reveals that they are a slowly varying function of frequency and increase as the size of the transverse mode indices (m, n, p, and t) increase.

By making a transformation of coordinates from cylindrical to Cartesian in (3) the expressions for lowest-order LG modes become identical to the lowest-order HG modes. Specifically,

$$\begin{aligned} &\mathrm{HG}_{00} = \mathrm{LG}_{00}, \quad \mathrm{HG}_{10} = \mathrm{LG}(cosine)_{01}, \\ &\mathrm{HG}_{01} = \mathrm{LG}(sine)_{01} \quad \text{and} \\ &\mathrm{HG}_{11} = \mathrm{LG}(sine)_{02}. \end{aligned} \tag{6}$$

Higher-order HG and LG modes are distinct.

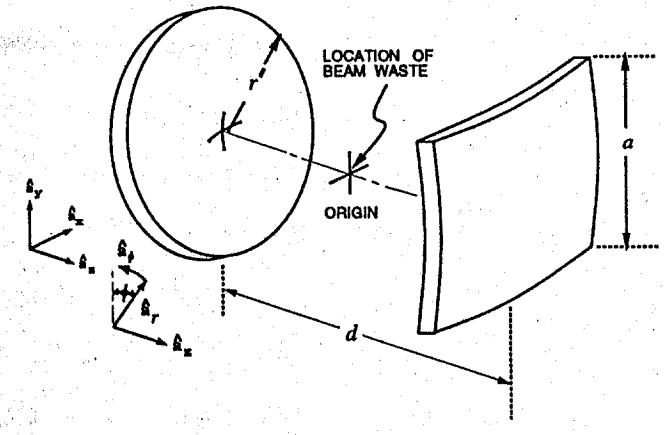

Figure 1 Nonconfocal Fabry-Perot resonator geometry

IV. EXPERIMENTAL INVESTIGATION

A planoconcave resonator was constructed using a circular aperture reflector of spherical cross section together with a rectangular plate reflector. This geometry supports half the number of possible modes as compared to a resonator with two curved reflectors because the planar reflector shorts out

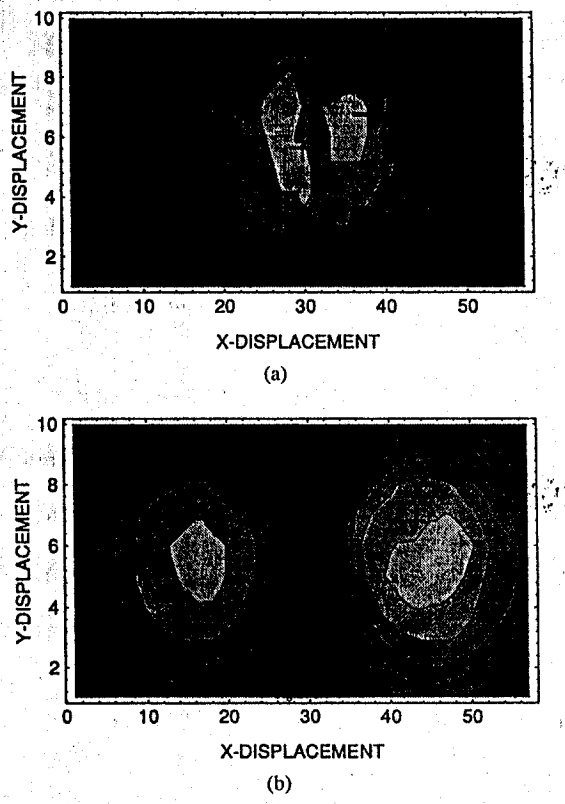

Figure 2 Measured 10 percentile contours of (a) the resonant $TEM_{0,0}$ mode at 8.503 GHz, and (b) the resonant $TEM_{1,0}$ mode at 8.552 GHz. The center axis of the resonator is indicated by the cross and the antenna by the bar. The axes scales indicate the sample index, and the sample spacing is 4.6 mm and 14.4 mm in the x and y directions

modes that would otherwise have had tangential electric fields at the beam waist. A circular aperture size of 55 cm in diameter was selected to create low losses for X-band longitudinal modes while providing mode selection through higher losses for transverse modes. The fields were mapped by exciting the cavity with a low-profile nonresonant inverted-L antenna and measuring the perturbation of the reflection coefficient by a small absorber placed in the field.

Profiles of the HG_{00} and HG_{10} modes are shown in Figure 2. These data are in close agreement with the profiles as indicated by (4) with the perturbation near the antenna attributed to near-field effects. Higher-order modes were detectable, but the relative magnitudes of these modes decreased rapidly with increasing mode index.

V. CONCLUSION

This article has demonstrated that the low-order mode structure of a quasioptical resonant can be approximated by either Hermite Gaussian or Laguerre Gaussian functions independent of aperture geometry. Higher-order modes are eliminated by limiting the size of the apertures. Furthermore, quasioptical system components can be designed to optimize impedance mode matching without regard to excitation of undesired modes.

ACKNOWLEDGMENTS

This work was supported by the U.S. Army Research Office through Grant No. DAAL03-89-D-0030.

REFERENCES

1. G. D. Boyd and H. Kogelnik, "Generalized Confocal Resonator Theory," *Bell Syst. Tech. J.*, July 1962, pp. 1347–1369.
2. T. Li, "Mode Selection in an Aperture-Limited Concentric Maser Interferometer," *Bell Syst. Tech. J.*, Nov. 1963, pp. 2609–2620.
3. M. Abramowitz and I. Stegun, *Handbook of Mathematical Functions*, Dover, New York, 1972.

Received 10-25-94

Microwave and Optical Technology Letters, 8/5, 230–232

CCC 0895-2477/95

COHERENT OPTICAL PROCESSOR FOR INVERSE FILTER GENERATION

Mustafa A. G. Abushagur and Vahid R. Riasati
Department of Electrical and Computer Engineering
University of Alabama in Huntsville
Huntsville, Alabama 35899

KEY TERMS

Optical processing, optical computing, Fourier optics

ABSTRACT

A new algorithm and system architecture for inverse filter generation using a coherent iterative optical processor is presented. This processor avoids the singularity problem usually faced in inverse filter generation. The algorithm convergence is analyzed and a convergence condition is derived. Computer simulation of the algorithm performance is presented, and the results confirm the theoretical predictions for the convergence. Two optical architectures for the implementation of this algorithm are also introduced, based on space- and time-domain utilization. © 1995 John Wiley & Sons, Inc.

I. INTRODUCTION

Optical processing and computing are emerging as major fields of interest that exploits the inherent advantages of optics. Systems can directly implement and utilize addition, multiplication, and Fourier transforming to perform variety of operations, some of which include linear algebra processing [1], correlation and convolution [2], spectrum analysis [3, 4], inverse filter generation, et cetera. In particular, the Fourier-transforming properties of optical systems can be utilized in the inverse filter problem. A number of articles have been published on the direct use of Fourier-transforming optical systems for the generation of inverse filters [5, 6]. Some of these use optical multiplication in the Fourier domain of two photographic plates. This, along with nonperfect imaging systems, impose stringent requirements on the development of optical inverse filters [7].

This article presents a new approach for inverse filter generation using an iterative method, rather than the direct use of the Fourier-transforming property of optics. In Section II we introduce the algorithm and derive the condition for convergence. In Section III, two designs for the coherent optical implementation of the algorithm are presented and discussed. The results of a computer simulation of the system using a typical optical frequency response function are presented in Section IV. And finally, Section V provides a brief discussion, some conclusions, and possible applications of the algorithm.